not allow us to determine the adsorption sites of the molecules.
21. K. Motai *et al.*, *Jpn. J. Appl. Phys.* **32**, L450 (1993); E. I. Altman and R. J. Colton, *Surf. Sci.* **295**, 13 (1993).
22. This method reduces the contribution of noise in imaging, as the tip displacements are well under the (1/6 maximum) difference between the 1/3 maximum threshold value and the half maximum at the perimeter of the area analyzed. The uncertainties reported are one standard deviation when tens of observations of each equivalent site are averaged. The occupation fractions measured are not particularly sensitive to the choice of areas and thresholds, so long as the STM topography due to a benzene molecule would be higher than the threshold for the area selected.
23. We do not have sufficient statistics to determine the order of these kinetics. Further, once the tunneling conditions are found that do not perturb the motion of the molecules, one can measure the occupation of the sites to much shorter times by following the tunneling current when the tip is kept fixed at the adsorption site.
24. D. L. Patrick, V. J. Cee, T. P. Beebe Jr., *Science* **265**, 231 (1994).
25. M. F. Crommie, C. P. Lutz, D. M. Eigler, *Nature* **363**, 524 (1993); Y. Hasegawa and Ph. Avouris, *Phys. Rev. Lett.* **71**, 1071 (1993); Ph. Avouris and I.-W. Lyo, *Science* **264**, 942 (1994).
26. M. M. Kamna, S. J. Stranick, P. S. Weiss, in preparation.
27. S. J. Lombardo and A. T. Bell, *Surf. Sci. Rep.* **13**, 1 (1991); D. L. Meixner and S. M. George, *J. Chem. Phys.* **98**, 9115 (1993).
28. We thank B. Bent, M. Cole, E. Heller, and H. Rohrer for helpful discussions. This research was supported by the National Science Foundation Chemistry and Presidential Young Investigator programs, the Office of Naval Research, AT&T Bell Laboratories, the Biotechnology Research and Development Corporation, Eastman Kodak, and Hewlett-Packard. S.J.S. thanks the Shell Foundation for a graduate fellowship.

6 June 1994; accepted 9 August 1994

Direct Determination of Grain Boundary Atomic Structure in $SrTiO_3$

M. M. McGibbon,* N. D. Browning, M. F. Chisholm, A. J. McGibbon, S. J. Pennycook, V. Ravikumar, V. P. Dravid

An atomic structure model for a 25° [001] symmetric tilt grain boundary in $SrTiO_3$ has been determined directly from experimental data with the use of high-resolution *Z*-contrast imaging coupled with electron energy loss spectroscopy. The derived model of the grain boundary was refined by bond-valence sum calculations and reveals candidate sites for dopant atoms in the boundary plane. These results show how the combined techniques can be used to deduce the atomic structure of defects and interfaces without recourse to preconceived structural models or image simulations.

Internal interfaces, such as grain boundaries, have a pervasive influence on a variety of macroscopic properties and phenomena (*1*). Although it is well accepted that the atomic structure of interfaces does dictate the behavior of the bulk, the details of this relation are far from clear. One such model electroceramic system in which grain boundary phenomena control a variety of electrical properties, such as nonlinear current-voltage characteristics (*2*, *3*) is $SrTiO_3$. The explanation for the electrical activity of grain boundaries is largely phenomenological, and there is considerable debate whether the electrical properties can be rationalized in terms of acceptor states at the grain boundary core (*4*–*6*). Thus, determining the atomic structure-property relation for individual grain boundaries in such systems is of considerable significance (*7*, *8*). As a first step toward this goal, we have initiated a study of $SrTiO_3$ bicrystals that limits the number of degrees of freedom associated with the interface and provides a realistic opportunity to probe the structure-property relation for single isolated boundaries (*9*).

To determine the atomic and electronic structure of the grain boundary on an atomic scale, a technique is required that probes both composition and chemical bonding with atomic resolution. Here we present a detailed atomic structure model for an undoped grain boundary in $SrTiO_3$, made possible by combining high-resolution Z-contrast imaging to locate the cation columns at the boundary, with simultaneous electron energy loss spectroscopy to examine light-element coordination at atomic resolution.

High-resolution Z-contrast imaging in the scanning transmission electron microscope (STEM) provides an incoherent image in which changes in atomic structure and composition across an interface can be interpreted directly without the need for preconceived atomic structure models (*10*). Provided the incident electron probe is smaller than the lattice spacing (for a sample oriented to a major zone axis), the current can be channeled along a single atomic column. Because the probe is scanned, the resultant image is a map of the columnar scattering power that in turn depends on the atomic number, Z, of each column. The spatial resolution is primarily limited by the probe size of the STEM [2.2 Å in our case, using a VG Microscopes HB501UX (Sussex, United Kingdom)] because beam spreading is reduced, even in thicker samples, by the channeling effect (*11*, *12*). Because the Z-contrast image is formed by electrons scattered through high angles, parallel detection electron energy loss spectroscopy (PEELS) can be used simultaneously to provide complementary chemical information on an atomic scale (*13*, *14*). The fine structure in the energy loss spectra can be used to investigate the local electronic structure and the nature of the bonding across the interface (*15*, *16*).

The power of combining Z-contrast imaging and PEELS to solve the atomic and chemical structure of grain boundaries is demonstrated here in the study of an undoped $SrTiO_3$ bicrystal purchased from Shinkosha, Ltd., Tokyo, Japan. Specimens with the boundary parallel to the beam direction were prepared for electron microscopy by mechanical polishing and ion-beam thinning. Figure 1A shows a Z-contrast image from a symmetric portion of a 25° [001] tilt boundary. At room temperature, $SrTiO_3$ has a cubic perov-

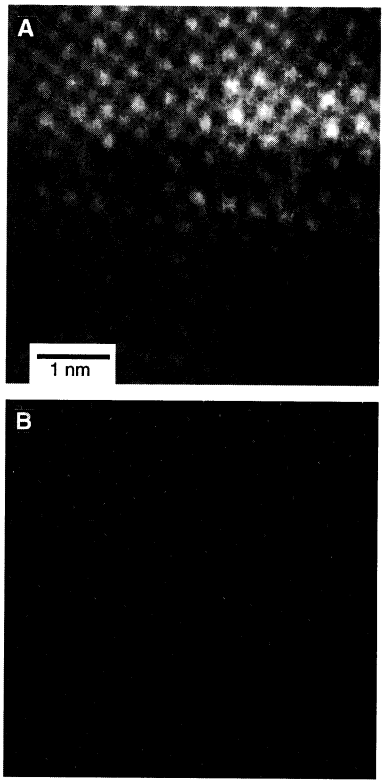

Fig. 1. (**A**) *Z*-contrast image of a 25° [001] tilt boundary in an $SrTiO_3$ bicrystal, with (**B**) the maximum entropy object function providing scattering intensities and coordinates of the Sr and Ti atomic columns directly from the image.

M. M. McGibbon, N. D. Browning, M. F. Chisholm, A. J. McGibbon, S. J. Pennycook, Solid State Division, Oak Ridge National Laboratory, Oak Ridge, TN 37831–6030, USA.
V. Ravikumar and V. P. Dravid, Northwestern University, Department of Materials Science and Engineering, Evanston, IL 60208, USA.
*To whom correspondence should be addressed.

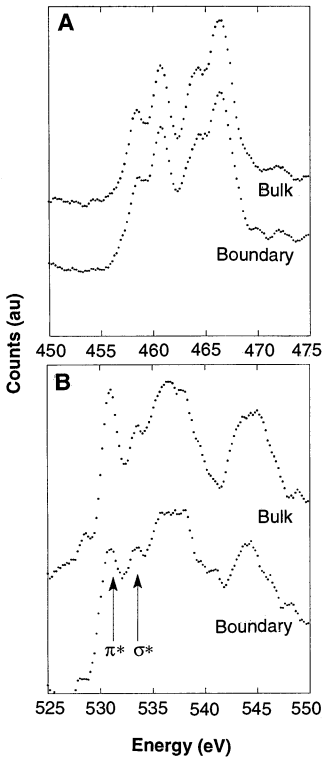

Fig. 2. A comparison of (**A**) Ti L_{23} spectra and (**B**) O K edge spectra acquired at the grain boundary and in the bulk of an $SrTiO_3$ bicrystal, showing that the octahedral Ti-O coordination is maintained across the boundary. Both the Ti and O spectra have been smoothed.

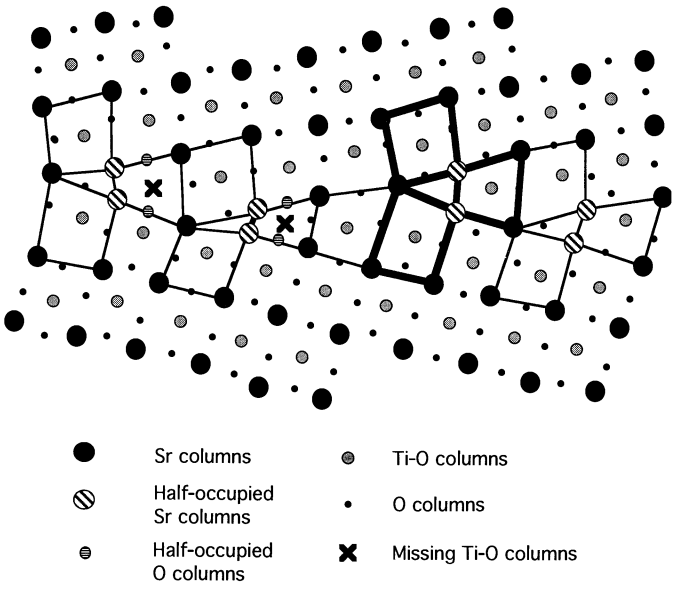

Fig. 3. A repeat unit of the grain boundary structure model determined by a combination of the structural information from the *Z*-contrast image and the Ti-O coordination deduced from PEELS. The O atom positions were refined by bond-valence sum calculations evaluated over all atoms shown.

skite structure (space group Pm3m) with a lattice parameter of 3.905 Å. The brighter spots in the image correspond to the strongly scattering Sr columns (Z = 38), with the less bright spots corresponding to the lighter Ti-O columns (Z = 22 for Ti and 8 for O). The pure O columns are not visible. We applied the maximum entropy image analysis technique (*17*, *18*) to Fig. 1A to enhance its resolution and to determine the positions and intensities of each atomic column from the image (Fig. 1B) (*19*). The coordinates of the Sr and Ti-O columns are determined directly from the maximum entropy object function without the need for a reference atomic model, as is necessary in other structure determination techniques such as phase contrast high-resolution electron microscopy and x-ray diffraction. The error associated with the determination of individual atomic coordinates was ~5% (0.2 Å). In addition, we estimate a systematic error of ~0.2 Å due to a 10-mrad tilt between the two halves of the bicrystal. This tilt effect and changes in specimen thickness result in the long-range variations in the intensity of the Z-contrast image shown in Fig. 1A. However, the short-range variations in intensity due to differences in the scattering cross section between the Sr and Ti-O columns always remain intuitive on the local scale.

The misorientation between the two grains in the bicrystal was measured directly from the Sr and Ti column coordinates (Fig. 1B) to be 25° ± 1°. The boundary is symmetrical with a (920)-type boundary plane common to both crystals, which corresponds to a $\Sigma = 85$ (920) symmetrical tilt grain boundary in coincident site lattice notation. The Sr and Ti-O column coordinates in the maximum entropy object function of Fig. 1B give direct information on the rigid body translation and the grain boundary expansion present at this interface. No in-plane rigid body shift is observed along the common (920) boundary plane within the 0.2 Å accuracy of the atomic column positions. By constructing a series of corresponding (920) planes in each unit cell across the grain boundary, we measured an expansion of 0.6 ± 0.2 Å normal to the boundary plane (*20*). Any distortions from cubic symmetry visible in the bulk lattice are due to an image artifact and are not real shear distortions in the crystal.

Whereas the coordinates of the Sr and Ti-O columns can be determined directly from the Z-contrast image, there is no information on the position of the O columns. However, use of the Z-contrast image to position the probe accurately at the grain boundary for simultaneous PEELS acquisition allows the fine structure within the PEELS edges to be used to investigate the O and Ti bonding at the boundary (*20*). Series of Ti and O spectra were acquired at unit cell intervals (~4 Å) across the $SrTiO_3$ grain boundary. To reduce the dose on a single atomic column, the spectra were acquired while the probe was rapidly scanned along a line parallel to the interface, thus retaining atomic resolution normal to the interface. The exposure time for the Ti L_{23} edge was limited to 2 s and for the O K edge it was limited to 5 s to minimize specimen drift (~2 to 3 Å/min). By collecting two spectra at each point it was possible to determine that no beam damage occurred during acquisition, allowing the spectra to be summed to improve counting statistics.

The Ti L_{23} and O K edges acquired in the bulk and at the grain boundary are compared in Fig. 2. The first peak of each edge arises from transitions to a π^* anti-bonding level between O 2p and Ti three-dimensional states, and the second peak arises from transitions to a σ^* anti-bonding level (*21*). Previous studies have shown that the Ti L_{23} fine structure is sensitive to the Ti coordination (*22*). Because we probed the unit cells forming the boundary plane and found no significant change, we conclude that the Ti atoms remain octahedrally coordinated to O across the grain boundary. The broadening of the π^* and the σ^* peaks at the boundary reflects a broadening of the corresponding energy levels due to distortion of the Ti-O bonds across the grain boundary. In addition, because no chemical shift is observed in the Ti edge onset in Fig. 2A, we conclude that the Ti valency in $SrTiO_3$ remains 4+ across the grain boundary region (*23*, *24*). In the O K edge spectra from the grain boundary (Fig. 2B) the increased σ^* intensity relative to π^* may also be attributed to the disrupted linear Ti-O coordination across the boundary (*25*). Therefore, we conclude that although the O-Ti-O bonds are distorted across the boundary plane, Ti remains octahedrally coordinated by O.

By combining this information on Ti-O coordination with the Sr and Ti-O column positions determined from the Z-contrast image, one can propose a model for the grain boundary structure (Fig. 3) directly from the experimental evidence. The grain boundary repeat structure consists of four triangular Sr subunits (shown in bold in Fig. 3) separated by a single distorted $SrTiO_3$ unit cell. Note the close proximity of the

hatched Sr columns in the Sr subunits, which are significantly below the lowest Sr-Sr distances commonly found in other compounds. The presence of these two Sr columns cannot be explained by factors such as specimen tilt or grain boundary steps, which indicates that these columns cannot be fully occupied. This observation is consistent with the reduced density at the grain boundary noted in studies by Merkle and Smith (*26*) in NiO and by Fonda and Luzzi (*27*) in NiAl. The simplest explanation is that each column is alternately occupied through the thickness of the sample because this occupation preserves the Sr-Sr spacing at ~4 Å. Because the Z-contrast image is incoherent it would still image two distinct atomic columns in such a case, each having reduced intensity, as is found experimentally. However, it is not possible to obtain precise atomic column occupancies directly from their intensities because of a number of second-order effects near the boundary plane (*28*). In addition, two of the four subunits in Fig. 3 contain missing Ti-O columns. These Ti and O vacancies appear to occur randomly in all of the symmetric regions of the grain boundary studied, and an equal population of subunits with and without the Ti-O columns preserves grain boundary stoichiometry. No evidence of structural multiplicity was observed in any of the symmetric regions of the grain boundary examined.

To test the validity of this observation and the proposed structural model, bond-valence sum calculations were performed (*29*, *30*). In these calculations, the contribution of a particular bond to the formal valence of each of the atoms involved in the bond is calculated from the bond length. With the coordinates of the metal columns determined from the maximum entropy object function, the oxygen column positions were refined to maintain charge neutrality with the correct valence on all the atoms. We have assumed the atoms to be confined to their respective {001} planes. It was necessary, in isolated cases, to adjust the positions of the metal columns to ensure that the valence on any individual site did not vary by more than 0.5 from the average valence. However, these movements were less than the 0.2 Å positional error in the coordinates, as can be seen from a comparison of the grain boundary structure model and the maximum entropy image (Fig. 4). In this manner, the average valencies and standard deviations in the structural unit were found to be 2.11 ± 0.23 for Sr, 4.08 ± 0.24 for Ti, and 2.08 ± 0.29 for O, which agree well with the values calculated for the bulk material [Sr = 2.11, Ti = 4.14, and O = 2.08, from the parameters given in (*29*)]. Although bond valence sums alone cannot determine the reason for the missing Ti-O columns, the Ti-O columns in the adjacent unit cells relax, which is consistent with preserving charge neutrality at the grain boundary.

The combination of the cation coordinates obtained from the Z-contrast image with the Ti-O coordination from PEELS allows a grain boundary structure model to be derived directly from experimental data. The position of the O atoms in this model structure were then refined with bond-valence sum calculations. The half-occupied Sr columns represent attractive sites for large dopants that substitute for Sr, whereas the Ti and O vacancies are likely sites for smaller dopant atoms. Because the surrounding atoms are seen to relax to accommodate the presence or absence of the Ti-O columns, these sites could accommodate dopants of different valence. Our model could form the basis of a detailed theoretical investigation of such possibilities, and the role of dopants and processing in the development of the grain boundary potential barriers could then be examined. We believe that further structural studies in conjunction with electrical characterization could finally elucidate the structure-property relations for grain boundaries in electronic ceramics.

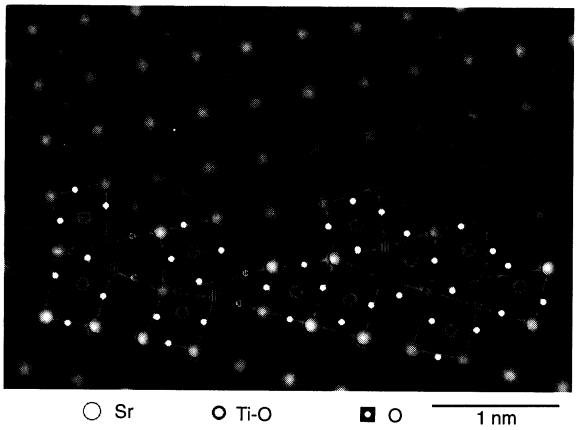

Fig. 4. The grain boundary structure model of Fig. 3 overlain the maximum entropy image (the object function convoluted with a narrow Gaussian). The half-occupied Sr columns (hatched circles) and Ti-O column vacancies provide candidate sites for dopant atoms.

REFERENCES AND NOTES

1. *Interfaces: Structure and Properties*, S. Ranganathan, C. S. Pande, B. B. Rath, D. A. Smith, Eds. (Trans Tech Publications, Aedemannsdorf, Switzerland, 1993).
2. N. Yamaoka, M. Masuyama, M. Fukai, *Am. Ceram. Soc. Bull.* **62**, 698 (1983).
3. M. Fujimoto and W. D. Kingery, *J. Am. Ceram. Soc.* **68**, 169 (1985).
4. P. Gaucher, R. L. Perrier, J. P. Ganne, *Adv. Ceram. Mater.* **3**, 273 (1988).
5. Y.-M. Chiang and T. Takagi, *J. Am. Ceram. Soc.* **73**, 3286 (1990).
6. S. B. Desu and D. A. Payne, *ibid.*, p. 3391.
7. E. Olsson and G. L. Dunlop, *J. Appl. Phys.* **66**, 4317 (1989).
8. D. A. Bonnell and I. Solomon, *Ultramicroscopy* **42–44**, 788 (1992).
9. V. Ravikumar and V. P. Dravid, *ibid.* **52**, 557 (1993).
10. S. J. Pennycook, *Annu. Rev. Mater. Sci.* **22**, 171 (1992).
11. ——— and D. E. Jesson, *Phys. Rev. Lett.* **64**, 938 (1990).
12. ———, *Ultramicroscopy* **37**, 14 (1991).
13. A. V. Crewe, J. Wall, J. Langmore, *Science* **168**, 1338 (1970).
14. N. D. Browning, M. F. Chisholm, S. J. Pennycook, *Nature* **366**, 143 (1993).
15. P. E. Batson, *ibid.*, p. 727.
16. D. A. Muller, Y. Tzou, R. Raj, J. Silcox, *ibid.*, p. 725.
17. S. F. Gull and J. Skilling, *IEEE Proc. F* **131**, 646 (1984).
18. A. J. McGibbon and S. J. Pennycook in *Proceedings of the 52nd Microscopy Society of America Conference*, New Orleans, LA, 31 July to 5 August 1994 (San Francisco Press, San Francisco, CA, 1994).
19. As a result of the spatial incoherence in the transverse plane, *Z*-contrast imaging can be described in terms of a convolution between an object function (the real-space map of the columnar scattering intensity to high angles) and the effective electron probe. The maximum entropy method of Gull and Skilling (*17*) calculates the most likely object function that, when convoluted with the effective probe, best matches the experimental data. The probe profile is the only additional information required by the program.
20. M. M. McGibbon *et al.*, *Mater. Res. Soc. Symp. Proc.* **341**, 139 (1994).
21. L. A. Grunes, R. D. Leapman, C. N. Wilker, R. Hoffman, A. B. Kunz, *Phys. Rev. B* **25**, 7157 (1982).
22. R. Brydson, H. Sauer, W. Engel, in *Transmission Electron Energy Loss Spectrometry in Materials Science* (*The Minerals*, Metals and Materials Society, Warrendale, PA, 1992), pp. 131–154.
23. J. H. Paterson and O. L. Krivanek, *Ultramicroscopy* **32**, 319 (1990).
24. M. T. Otten, B. Miner, J. H. Rask, P. R. Busek, *ibid.* **18**, 285 (1985).
25. R. Brydson, H. Sauer, W. Engel, F. Hofer, *J. Phys. Cond. Matter* **4**, 3429 (1992).
26. K. L. Merkle and D. J. Smith, *Phys. Rev. Lett.* **59**, 2887 (1987).
27. R. W. Fonda and D. E. Luzzi, *Philos. Mag. A* **68**, 1151 (1993).
28. These include uncertainties in the validity of the Einstein model for thermal diffuse scattering, a possible change in the atomic vibration amplitude for atoms in the boundary plane, and disorder scattering and dechanneling effects due to surface relaxation of strained regions near the boundary.
29. D. Altermatt and I. D. Brown, *Acta Crystallogr.* **B41**, 240 (1985).
30. I. D. Brown and D. Altermatt, *ibid.*, p. 244.

31. We thank B. C. Chakoumakos and F. A. Modine for helpful discussions and T. C. Estes, J. T. Luck, and S. L. Carney for technical assistance. Supported by the Division of Materials Sciences, U.S. Department of Energy, under contract DE-AC05-84OR21400 with Martin Marietta Energy Systems, and an appointment to the Oak Ridge National Laboratory Postdoctoral Research Program administered by the Oak Ridge Institute for Science and Education. V.R. and V.P.D. are supported by U.S. Department of Energy grant DE-FG02-92ER45475.

16 May 1994; accepted 22 August 1994